Zymogen granule exocytosis is characterized by long fusion pore openings and preservation of vesicle lipid identity

Peter Thorn*†, Kevin E. Fogarty‡, and Ian Parker§

§Department of Neurobiology and Behavior, University of California, Irvine, CA 92697; ‡Department of Physiology, Biomedical Imaging Group, University of Massachusetts Medical School, Worcester, MA 01650; and *Department of Pharmacology, University of Cambridge, Tennis Court Road, Cambridge CB2 1PD, United Kingdom

Edited by Pietro De Camilli, Yale University School of Medicine, New Haven, CT, and approved March 1, 2004 (received for review January 15, 2004)

The dynamics of the fusion pore that forms between a secretory vesicle and the plasma membrane are important in the regulation of both exocytosis and endocytosis. Here, we describe characteristics of fusion during zymogen granule exocytosis in exocrine pancreatic acinar cells. By using fluorescence recovery after photobleaching techniques, we show that the fusion pore remains open to allow free aqueous exchange with the vesicle lumen. There is no lipid interchange between the plasma and granule membranes during this time, and at the end of its life, the intact granule shrinks *in situ*, probably by a gradual pinching off of membrane patches. We propose that the protracted fusion pore lifetime is adapted to permit compound exocytosis, whereby the lingering primary granule acts as a conduit through which the contents of a secondary granule can be released. The lack of lipid intermixing may then facilitate selective recycling of granule membrane and preservation of apical membrane integrity.

The culminating steps of exocytosis involve the interaction of proteins in the vesicle and plasma membranes to form an aqueous connection, the fusion pore, between the vesicle lumen and the extracellular space. Although many molecular components of the fusion pore complex are well characterized, we are only beginning to understand its mechanistic behavior during exocytosis. A striking feature is the variability of mechanisms and kinetics among different cell types (1). In some, vesicle fusion involves the intermingling of the vesicle and plasma membrane lipids leading to incorporation of the vesicle into the plasma membrane ("kiss and collapse") (2–4). In other cells, vesicle fusion does not lead to lipid interchange. Instead, the vesicle is recaptured intact by endocytotic processes so that it can then be refilled and recycled in another round of exocytosis ("kiss and run") (5–8). The latter process requires a stable fusion pore complex that prevents vesicle collapse and that is maintained sufficiently long enough to allow the vesicle to be pinched back (8–9).

The characteristics of exocytosis and endocytosis in acinar cells of exocrine pancreatic glands (10, 11) involve compound exocytosis (10,11) from secretory vesicles (zymogen granules) that display extraordinarily long lifetimes (11), and it is not clear whether the above models of exocytosis are applicable in these cells. Our experiments reveal that the fusion pore remains open for extended periods, and there is no lipid interchange between the granule and the plasma membrane: specializations that may facilitate compound exocytosis and selective recycling of vesicle membrane.

Materials and Methods

Cell Preparation. Intact lobules and fragments of mouse pancreas were prepared by collagenase digestion method in normal NaCl-rich extracellular solution (12), modified to reduce the time in collagenase and limit mechanical trituration. The resulting preparation was composed mainly of pancreatic lobules and fragments (≈50–100 cells), which were plated onto poly-L-lysine-coated glass coverslips.

Two-Photon Imaging. We used a custom-made, video rate, two-photon microscope (13, 14) with a 40× oil-immersion objective (N.A. 1.35, Olympus), providing a resolution (full width at half maximum) of 0.26 μm lateral and 1.3 μm axial. Images (resolution of 8–19 pixels·μm^{-1}, averaged 12–45 video frames) were analyzed with the METAMORPH program (Universal Imaging, Downington, PA). An epifluorescent mercury light source provided UV light to photolyse caged compounds within a ≈100-μm diameter field at the image plane. High-resolution image stacks of single zymogen granules (Fig. 2*A Inset*) were processed by using a custom image deconvolution program (15). Event kinetics were measured from regions of interest (0.39 μm^2, 100 pixels) over granules. Background fluorescence was subtracted and traces were normalized either to the peak or plateau fluorescence signal. We observed no appreciable photobleaching over time, and traces were rejected if movement was observed.

Fluorescent Probes. We imaged exocytotic events by using sulforhodamine (SRB; 500 μM) or Oregon green 488 1,2-bis(2-aminophenoxy)ethane-*N*,*N*,*N*′,*N*′-tetraacetate (BAPTA-1) (OG; 100 μM) as membrane-impermeant fluorescent extracellular markers. Dyes were excited by femtosecond laser pulses at 780 nm, with fluorescence emission detected at respective wavelengths of 550–650 nm and <550 nm, respectively. To stimulate exocytosis, we added 20 μM caged carbachol (CCh) to the bathing medium and adjusted the duration (0.1–5 s) of UV photolysis flashes to evoke infrequent exocytotic events in each cell.

Fluorescence signals were monitored from membranes by using the lipophilic dyes Calcium green C18 (CaG-C18; 20 μM) or FM1–43 (5 μM). CaG-C18 was excited at 780 nm and monitored at 515–565 nm, while simultaneously monitoring SRB fluorescence at 620–650 nm. In experiments with FM1–43, we excited at 820 nm and collected the emitted light through a 535 ± 20-nm bandpass filter while simultaneously collecting the SRB fluorescence at 620–650 nm. Although FM1–43 and SRB have some overlap in their emission spectra, these filter sets effectively isolated the FM1–43 fluorescence (< 5% bleed of SRB signal into the FM1–43 channel). Bleed in the opposite direction was unimportant, because the SRB signal was simply used as a marker for exocytotic events. Fluorescent probes and caged CCh were from Molecular Probes; all other compounds were from Sigma.

This paper was submitted directly (Track II) to the PNAS office.

Abbreviations: SRB, sulforhodamine B; OG, Orgeon green 488 1,2-bis(2-aminophenoxy)ethane-*N*,*N*,*N*′,*N*′-tetraacetate 1 (BAPTA-1); CaG-C18, calcium green C18; CCh, carbachol.

†To whom correspondence should be addressed. E-mail: pt207@cam.ac.uk.

www.pnas.org/cgi/doi/10.1073/pnas.0400336101

Confocal Imaging. Fluorescence recovery after photobleaching experiments in Fig. 3*D* were performed on a Zeiss LSM 510 confocal microscope with a 63× 1.4 N.A. planacromat oil-immersion objective. Bleaching was performed by using the Argon laser at full power over a 2.8-μm^2 area. The average fluorescence intensity over time within the bleach area was plotted and fitted to a single exponential (ORIGIN software).

Cell Fixation. For the experiments shown in Fig. 4*E*, cells were washed in PBS and were incubated in 4% paraformaldehyde (in PBS) for 30 min. They were then washed and were treated with 0.1% Triton X-100 for 5 min. After washing again, FM1–43 was applied and cells were imaged by confocal microscopy as above.

Results

Identification of Single Exocytotic Events. Lobules and fragments of mouse pancreatic tissue retained the typical exocrine morphology of a fine network of branching ducts, terminating at clusters of acinar cells. Inclusion of a fluorescent probe (SRB or OG) in the extracellular bathing medium labeled acini lumen and the extracellular space between cells, but both dyes were excluded from the cell interior (Fig. 1*A*). Two-photon microscopy provided a thin (≈1 μm) optical slice through the tissue and, because excitation is confined to the focal plane, out-of-focus fluorescence from the large volume of dye surrounding the preparation was minimized. Uncaging of CCh with a flash of UV light evoked fluorescence spots in the apical, but not basal, regions of cells (Fig. 1*A*, and Movie 1, which is published as supporting information on the PNAS web site). Control experiments omitting caged CCh showed no responses. The kinetics (Fig. 1 *B* and *C*), size (Fig. 1*D*), and apical localization of these fluorescent spots are consistent with extracellular dye entering single zymogen granules during exocytosis (10, 11, 16–18). We often observed that fusion of a granule to the plasma membrane was followed by granule–granule fusion, which is suggestive of compound exocytosis as well described in this cell (10, 11). Fig. 1*E* shows an example of sequential fusion leading to a chain of three granules. The distribution of latencies between primary and secondary granule events (Fig. 1*E*) fit an exponential (τ = 22.0 s), similar to that described (11).

The Fusion Pore Remains Open During Protracted Fusion Events. We studied individual primary events under conditions where only one or a few events were evident in each cell by using either weak photorelease of CCh or imaging infrequent spontaneous events (n = 48 events in total). Fluorescence measurements from regions of interest centered on granule events displayed a biphasic fluorescence signal (peak followed by plateau: e.g., Figs. 1*B* and 2*A*). The peak appears to represent binding of dye to intragranular contents that are lost over a period of a few seconds (P.T. and I.P., unpublished data). What is important here is the protracted persistence of the plateau phase (e.g., >10 min in Fig. 2*A*), pointing to the continued existence of an intact dye-filled granule.

We considered two explanations for the long plateau phase. The granule might retain dye after closing of the fusion pore, or it may remain in stable continuity with the duct lumen through an open fusion pore. To address this issue, we carried out two sets of experiments. We first collected high-resolution (0.1-μm axial steps) image stacks of granules during the plateau phase. Three-dimensional reconstructions of deconvolved images show Ω-shaped granules, with a narrow neck apparent between the granule and the duct (Fig. 2*A Inset*, and Movie 2, which is published as supporting information on the PNAS web site), supporting the idea of a physical link between the granule and the duct. In the second, with more definitive experiments, we bleached the dye in the granules and adjacent ducts by using pulses of intense light (λ = 440–480 nm) at various times after granule fusion. In all cases (n = 9 of 9, photobleaching between 18 and 161 s after event peak) we observed rapid (τ = 27.8 ± 7.5 s) and almost complete recovery of fluorescence, indicating that the granule remained in continuity with the extracellular environment and refilled with dye through an open pore (Fig. 2 *B* and *C*).

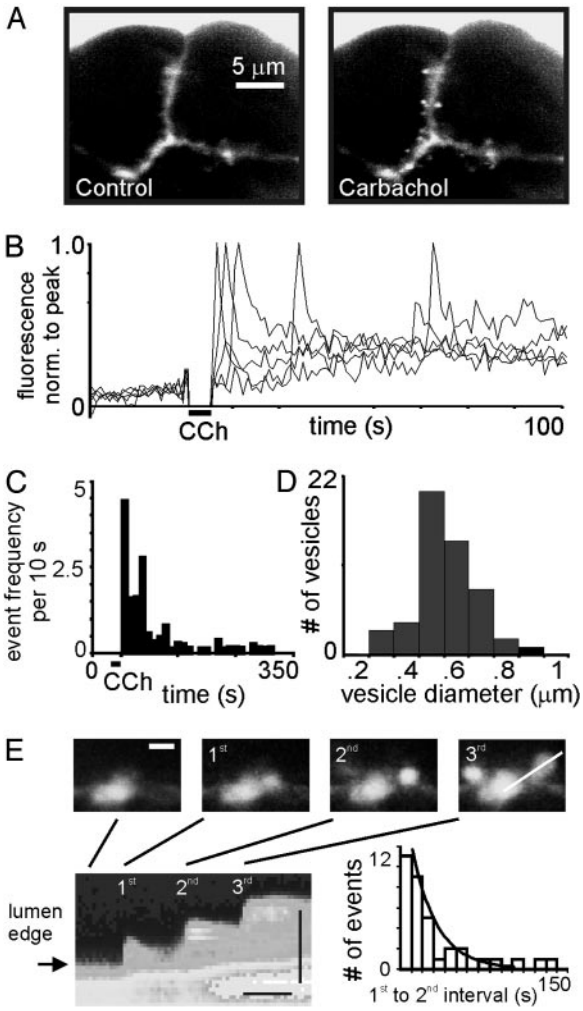

Fig. 1. Exocytotic events in pancreatic acini induced by photorelease of CCh. (*A Left*) A group of three cells on the edge of a pancreatic lobule, imaged by two-photon excitation of an extracellular marker dye (SRB). Fluorescence is apparent in the solution surrounding the cells, in the intercellular spaces, and in the acinar lumen (a ''tristar'' shape in the center). (*Right*) The same cells a few seconds after a flash of UV light to photolyse caged CCh (≈1 μM). Bright fluorescent spots in the apical domains of the cells mark granules that fused during exocytosis. (*B*) Superimposed traces show measurements of average fluorescence records over time from five regions of interest placed over event locations. Individual traces were normalized to the peak fluorescence. (*C*) Distribution of event latencies after CCh photorelease (nine independent preparations and 274 events) expressed as the average number of events per cell, per 10-s time bin, per optical slice. (*D*) Distribution of granule diameters, measured at full width at half maximum (0.51 ± 0.02 μm, mean ± SEM; n = 41). (*E*) Example of compound exocytosis. (*Upper*) A time series of successive events involving successive granule–granule fusion, leading to a chain of three fused granules extending deep into the cell. (Scale bar, 2 μm.) (*Lower*) A line scan image derived from this record by displaying fluorescence intensity along a line (vertical axis; scale bar, 2 μm) through the three vesicles (*Right Upper*) as a function of time (horizontal axis; scale bar, 10 s). Graph shows distribution of latencies between first- and second-granule events (n = 36 paired events). Curve is a single exponential with τ = 22s.

PHYSIOLOGY

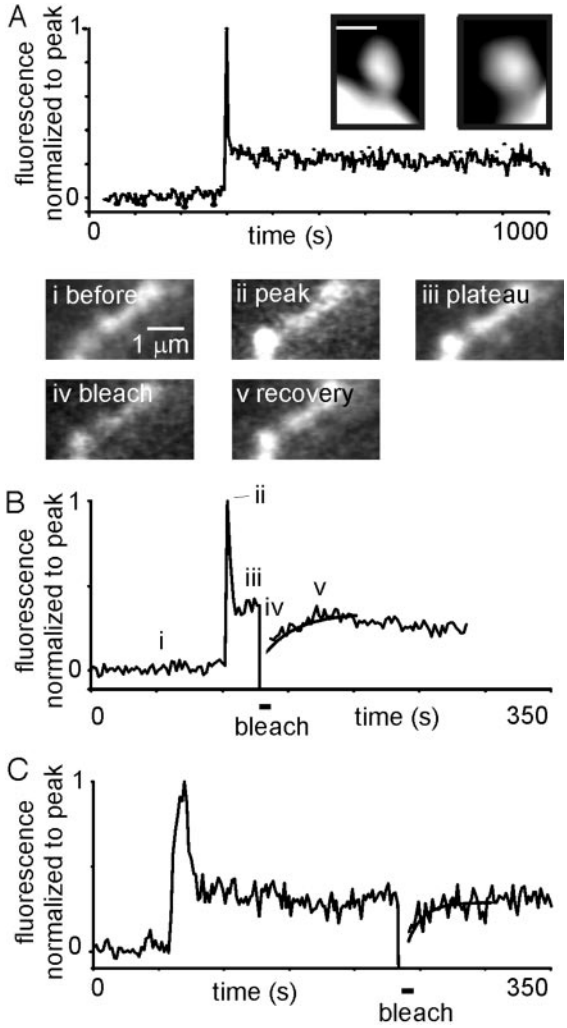

Fig. 2. Protracted fusion pore openings. (*A*) Trace shows the (OG) fluorescence signal during a representative vesicle–fusion event, demonstrating a biphasic signal with a protracted plateau, lasting several minutes. (*Inset*) Images were derived from two-photon *z* sections recorded during the plateau phase by deconvolution and 3D reconstruction. Orthogonal views show the vesicle apparently connected to an associated duct by a narrow neck. (scale bar, 0.5 μm) (*B*) Photobleaching of dye in the granule reveals maintained aqueous continuity between the granule lumen and duct during the plateau phase. The trace illustrates OG fluorescence monitored from a single-fusion event, and corresponding images were captured at times indicated on the trace. A flash of intense light (440–480 nm) was applied (horizontal bar) to photobleach dye in the granule and adjacent duct. The curve is an exponential fit, showing almost complete fluorescence recovery to the prebleach plateau level. (*C*) Another example, showing fluorescence recovery after bleaching later during the plateau phase of an exocytotic event.

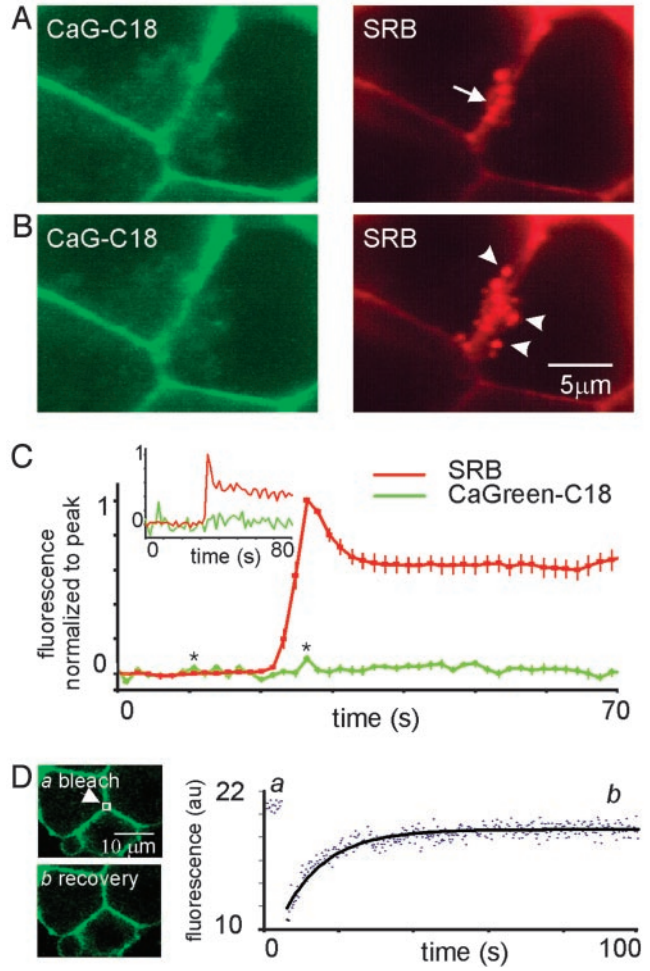

Fig. 3. Granule and plasma membranes do not intermingle during exocytosis. (*A*) Simultaneously acquired images showing fluorescence of CaG-C18 (green, stains plasma membrane) and SRB (red, stains extracellular spaces). Some preexisting fused granules are apparent in the SRB image, but not in the CaG-C18 image; arrow, acinar lumen. (*B*) Corresponding images obtained after uncaging CCh. Several newly fused granules are apparent in the SRB image (arrowheads show examples), but are not labeled by CaG-C18. (*C*) Traces show a representative single event (*Inset*), and mean measurements (± 1 SEM) of SRB (red trace) and CaG-C18 fluorescence (green) from 18 events (main plot). SRB traces were normalized to the peak, and CaG-C18 traces were normalized to fluorescence measured in the plasma membrane. Asterisks indicate time points where significance was tested for the CaG-C18 data. (*D*) Control experiment demonstrating mobility of CaG-C18 in the plasma membrane. Images were obtained before (*a*) and ≈80 s after (*b*) photobleaching a small region of membrane (arrowed box in *a*). Graph shows fluorescence recovery monitored from the bleached area, fitted by an exponential (τ = 11.46 s).

Zymogen Granule and Plasma Membranes Do Not Mix During Exocytosis. The sustained aqueous continuity between vesicles and the acini lumen raise the question of whether the lipid phase of the granular membrane also becomes contiguous with the plasma membrane. This issue has important consequences for the mechanisms of endocytosis, and for a recent model (11), suggesting that compound exocytosis requires the diffusion of exocytotic proteins from the plasma membrane into the granule membrane.

We thus looked for lipid interchange after granule fusion by preloaded the plasma membrane of pancreatic fragments with a lipophilic dye, and then by thoroughly washing out remaining aqueous extracellular dye before stimulating exocytosis. Thus, incorporation of dye in the granule membrane could occur only if there were lipid continuity with the plasma membrane. We initially tried the lipophilic marker FM1–43 (18, 19), but found this unsuitable because the dye washed out rapidly (half-time ≈20 s) from the plasma membrane. Instead, CaG-C18 gave optimal results. It remained in the plasma membrane for >30 min after washing, and its fluorescence emission could be could be clearly separated from that of SRB used simultaneously as a marker of granule fusion (Fig. 3*A*). After stimulation with CCh, numerous granules became apparent by SRB fluorescence, but we failed to observe any granule membrane labeling by CaG-C18 (Fig. 3*B*). Individual events showed no detectable signal during or after granule fusion, and even after averaging records from 18

events, the CaG-C18 signal remained flat (Fig. 3*C*; Student's *t* test, $P < 0.267$).

To verify that the lack of staining of granular membrane arose through a specific barrier to diffusion into the granule membrane rather than restricted mobility of CaG-C18 in the lipid membrane, we preloaded the plasma membrane with CaG-C18 as before, and we then photobleached small areas (2.8 μm^2) of plasma membrane (Fig. 3*D*). In all cases ($n = 9$), the fluorescence recovered almost completely after bleaching ($\tau = 9.2 \pm 1.39$ s), with no significant difference (Student's *t* test, $P = 0.195$) between recovery rates in the apical or basal pole. Thus, CaG-C18 is free to diffuse over micrometer distances in the plasma membrane on a time scale that is short, as compared with the granule lifetime.

As a final set of controls, we established that our imaging techniques were, indeed, sufficiently sensitive to detected labeling of the granule membrane if this had occurred. For this purpose, we imaged granule membranes stained by the lipophilic FM1–43 dye after its entry into the vesicle through the open fusion pore. As before, acini were stimulated with CCh, and exocytosis was monitored with SRB, but FM1–43 was now left in the extracellular medium throughout the experiment at a concentration that gave a plasma membrane fluorescence matching that in the CaG-C18 experiments (Fig. 4 *A* and *B*). In all cases ($n = 24$ of 24), CCh-evoked events showed an obvious and significant increase in the FM1–43 signal (Fig. 4*C*; Student's *t* test $P < 0.01$). Because FM1–43 becomes fluorescent only after partitioning into lipid, these signals most likely arose from FM1–43 in the granule membrane, to which it had access by means of aqueous entry through the fusion pore (20). In agreement, averaged images of fused vesicles showed FM1–43 staining around their edges, whereas the aqueous marker SRB showed maximum fluorescence in the center of the granule (Fig. 4*D*). This observation also argues against the possibility that the FM1–43 fluorescence may have arisen, owing to its binding to granule contents, as reported in other cell types (19, 21). Moreover, application of FM1–43 to fixed and permeabilized acinar cells showed staining of intracellular membranes, but exclusion from the granules (Fig. 4*E*, $n = 7$ cell clusters).

Postfusion Lifespan of Primary Zymogen Granules and Their Subsequent Endocytosis. There was considerable variability among vesicles in the duration of the plateau phase (Fig. 5*A*). In a few instances, fluorescence declined to the baseline almost immediately after the initial transient, but most events showed a prolonged plateau before the fluorescence began to drop (median duration 70 s: range 0 to 740 s; $n = 84$ events), and this value is underestimated because most events (57 of 84) persisted until the end of the recording period (3–15 min). In instances when event termination was captured, it was marked by a pronounced transition from a stable plateau fluorescence to a gradual decline that continued for tens of seconds before reaching the baseline. This decline was never accompanied by movement of the granule away from the plasma membrane or out of the region of interest. Instead, granules shrank gradually toward the membrane (Fig. 5*B*, $n = 33$ events).

This lack of granule movement indicates that endocytotic recycling does not involve retrieval of intact granules back into the cell. Instead, shrinkage of the granule might result either if the granule membrane fused into the plasma membrane, or if it were gradually endocytosed while remaining closely apposed to, but not in lipid continuity with, the plasma membrane. To discriminate between these possibilities, we again used CaG-C18 as a lipophilic marker to determine whether lipid interchange between plasma and granule membranes occurred during the end of the granule life. SRB was used to monitor the collapse of the vesicle, and Fig. 5*C* shows averaged records (six events) aligned relative to the times at which the plateau SRB fluorescence began to decay. No increase in CaG-C18 fluorescence was detectable, supporting the second of the above mechanisms.

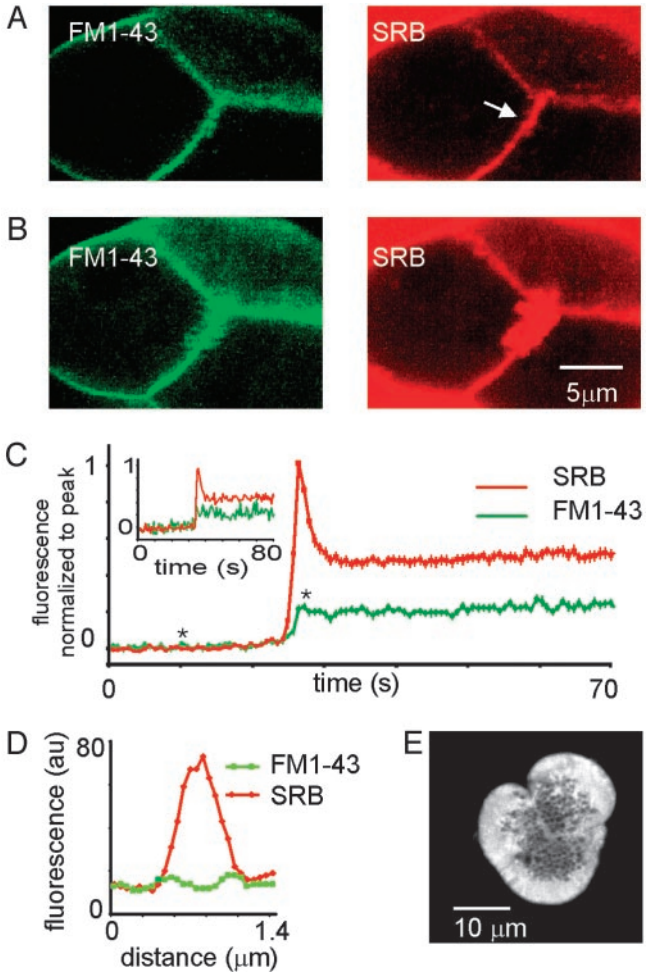

Fig. 4. Control experiments using the lipophilic dye FM1–43 demonstrate labeling of granule membrane. (*A*) Simultaneously acquired images showing fluorescence of the lipophilic dye FM1–43 (green, stains plasma membrane) and SRB (red, stains extracellular space). SRB and FM1–43 were present at all times in the extracellular medium; arrow, acinar lumen. (*B*) Entry of SRB into vesicles after CCh-induced exocytosis was accompanied by a rise in FM1–43 fluorescence. (*C*) Traces show a representative single event (*Inset*) and mean measurements (± SEM: main graph) of SRB and FM1–43 fluorescence from 24 events. Asterisks indicate times when significance was tested for the FM1–43 data. SRB traces were normalized to the peak, and FM1–43 traces were normalized to fluorescence measured in the plasma membrane. (*D*) Profiles of SRB and FM1–43 fluorescence measured along a scan line drawn through an averaged image of 28 granules. (*E*) A cluster of fixed, permeabilized acinar cells showing FM1–43 staining of intracellular membranes, but no staining of granule contents (dark spots in the apical domains).

Discussion

We describe distinct characteristics of zymogen granule exocytosis and endocytosis that may represent specific adaptations to support secretion in pancreatic acinar cells (Fig. 6). Long fusion pore open times permit protracted aqueous interchange between the granule lumen and extracellular fluid but, throughout this time, a barrier to interchange of lipids retains the granule membrane identity. Moreover, the endocytotic recycling of the granule membrane involves neither recapture of intact vesicles [kiss and run (1, 5–9)] nor collapse into the plasma membrane [kiss and collapse (2–4)]. Instead, our results are consistent with a piecemeal endocytotic retrieval of membrane direct from the

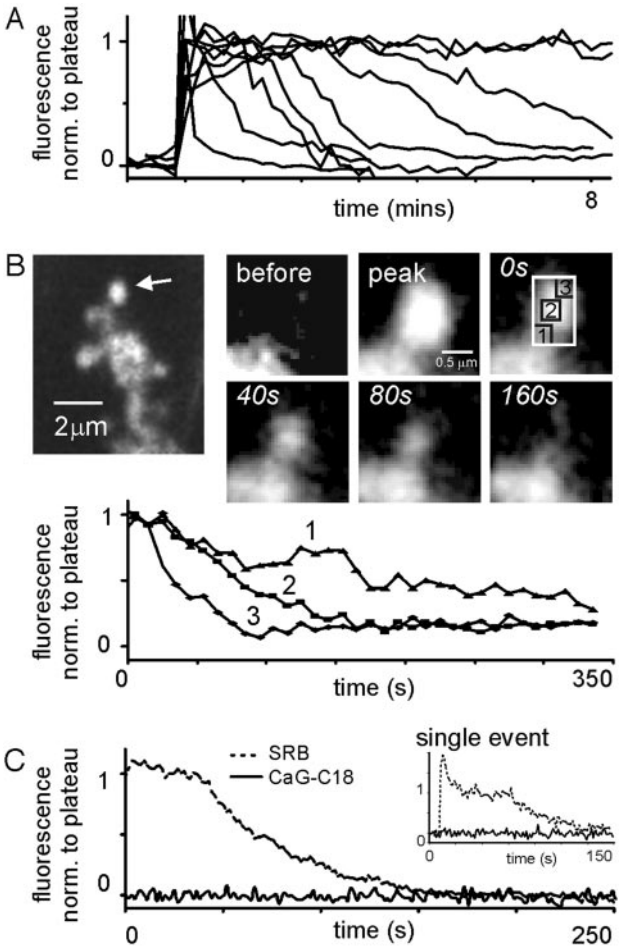

Fig. 5. Granule lifetimes and termination of fluorescence signals. (*A*) Superimposed traces show fluorescence records from nine representative events, displaying diverse granule lifetimes. Traces are normalized to the plateau amplitude and are aligned in time to their rising phases. Owing to the slow imaging rate, the initial peaks were not well resolved. (*B*) The decline in fluorescence at the end of the plateau phase is associated with shrinkage of the granule. The larger image (SRB fluorescence) is a low-magnification view of an acinar lumen showing a number of CCh-stimulated granule events. The sequence of images on the right show high-magnification views of the granule arrowed at left, at various times (indicated in s from end of plateau) during its lifetime. The graph shows measurements derived from the regions of interest shown in the image at 0 s. Traces are shown beginning from the time when fluorescence began to decline from the plateau and are normalized to the same initial intensities. (*C*) Lack of lipid interchange at the end of the granule lifetime. (*Inset*) Graph shows simultaneous measurements of SRB (dotted trace) and CaG-C18 fluorescence (solid trace) obtained as in Fig. 3 during the entire lifetime of an individual vesicle. The main graph shows mean measurements from six events, aligned relative to the onset of decay of SRB fluorescence from the plateau phase. Fluorescence intensities are scaled relative to the SRB fluorescence at the end of the plateau phase, CaG-C18 fluorescence intensities were scaled to the fluorescence measured at the plasma membrane.

intact zymogen granule. We conclude that these properties of zymogen granule secretion in acinar cells are specializations that support compound exocytosis and facilitate recycling of granule membrane and proteins, while maintaining the integrity of the apical plasma membrane.

We show that dye-filled primary granules persist for long times (median >70s, sometimes >12 min), which is consistent with previous observations (11), and further demonstrate by photobleaching, experiments that the fusion pore remains open for much, if not all of this time (at least 161 s; our longest test

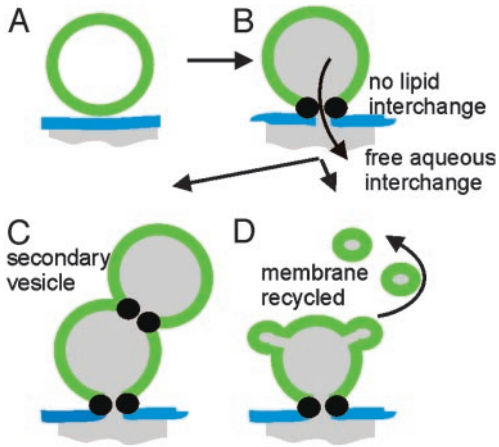

Fig. 6. Proposed cycle of exocytosis and endocytosis in acinar cells. Cartoon illustrates the following: (*A*) Granule before fusion; (*B*) Fused granule, with the fusion pore structure allowing continued aqueous interchange but acting as a barrier to intermingling of granule and plasma membranes; (*C*) Fusion of a secondary granule onto the persistent ghost of a primary vesicle by means of granule-associated fusion pore proteins; and (*D*) recycling of granule membrane by pinching back of patches from a primary ghost.

bleach). Similar photobleaching techniques have revealed similarly long fusion pore openings in alveolar type II cells (21). In those cells, vesicle contents are lost slowly, necessitating long fusion pore openings (21). However, granule contents are lost rapidly in pancreatic acinar cells (17) (P.T. and I.P., unpublished observations), suggesting the long openings subserve a different function.

Given the protracted aqueous continuity between zymogen granules and the extracellular space, how might the granule lipid be preserved? One possibility is that the proteinaceous fusion pore complex itself might form a barrier to lipid interchange. Because granule contents, such as amylase, are large molecules (20) (≈60 kDa), the fusion pore must be relatively large, and as such, may be stabilized by connections to cytoskeletal elements such as the actin cortex (22). Thus, accessory proteins, and not just proteins directly involved in the fusion pore complex, could form a barrier to lipid movement. Second, known differences in the lipid content of the granule and plasma membrane could act to segregate lipids in a manner analogous to lipid rafts in the plasma membrane (23). Finally, lipid diffusion rates are known to depend on membrane folding; it is possible that an acute angle formed between the plasma membrane and the granule membrane could act to limit lipid interchange (24).

Our observations that zymogen granules end their lifetime by slowly shrinking while maintaining their lipid identity (Fig. 5) are inconsistent with the dissolution of the fusion pore complex that precedes rapid vesicle collapse in kiss-and-collapse forms of exocytosis (2–4). Moreover, we found no evidence for retrieval of intact zymogen granules as in a kiss-and-run-type mechanism (1, 5–9, 25). We thus propose a route for endocytosis by the piecemeal retrieval of granule membrane from the zymogen granule (Fig. 6), as has previously been proposed on the basis of electron micrographs of salivary acinar cells showing small vesicles (≈50 nm) budding off from secretory granules (26–28). We now demonstrate this process in living cells and further show that granule lipid integrity is maintained during membrane retrieval.

An important likely function of long fusion pore openings is to permit compound exocytosis (10, 11), whereby a secondary granule fuses to a primary granule through which it releases its contents (Fig. 6*B*). Clearly, the fusion pore of the primary granule must remain open so that it can function as a conduit,

and the lack of lipid interchange with the plasma membrane may be crucial in maintaining the structural integrity of the primary granule. Moreover, this mechanism has other important implications. Previous work has suggested that diffusion of soluble *N*-ethylmaleimide-sensitive factor-attachment protein receptors from the plasma membrane into the membrane of the primary granule provides the necessary target for secondary granule fusion (11). The segregation of lipids we observe is likely to limit movement of proteins, and thus argues against such a model. In support of this hypothesis, *in vitro* experiments show that vesicle–vesicle fusion can take place independent of plasma membrane *N*-ethylmaleimide-sensitive factor-attachment protein receptors (29). The maintained separation of granule and plasma membranes may also facilitate recycling of granule lipids and proteins, as well as preserving the integrity of the highly specialized apical plasma membrane.

We thank Dr. C. Schwiening for assistance with the line scan images of Fig. 1, and Professor R. D. Burgoyne and Dr. Mike Edwardson for comments on the manuscript. This work was supported by The Wellcome Trust (P.T., I.P., and K.E.F.), United Kingdom Medical Research Council Project Grant G0000214 (to P.T.), and National Institutes of Health Grant GM48071 (to I.P.).

1. Valtorta, F., Meldolesi, J. & Fesce, R. (2001) *Trends Cell Biol.* **11,** 324–328.
2. Ceccarelli, B., Hurlbut, W. P. & Mauro, A. (1972) *J. Cell Biol.* **54,** 30–38.
3. Ryan, T. A., Smith, S. J. & Reuter, H. (1996) *Proc. Natl. Acad. Sci. USA* **93,** 5567–5571.
4. Zenisek, D., Steyer, J. A., Feldman, M. E. & Almers, W. (2002) *Neuron* **35,** 1085–1097.
5. Heuser, J. E. & Reese, T. S (1973) *J. Cell Biol.* **57,** 315–344.
6. Alvarez de Toledo, G., Fernandez-Chacon, R. & Fernandez, J. M (1993) *Nature* **363,** 554–558.
7. Alés, E., Tabares, L., Poyato, J. M., Valero, V., Lindau, M. & Alvarez de Toledo, G. (1999) *Nat. Cell Biol.* **1,** 40–44.
8. Holroyd, P., Lang, T., Wenzel, D., De Camilli, P. & Jahn, R. (2002) *Proc. Natl. Acad. Sci. USA* **99,** 16806–16811.
9. Graham, M. E., O'Callaghan, D. W., McMahon, H. T. & Burgoyne, R. D. (2002) *Proc. Natl. Acad. Sci. USA* **99,** 7124–7129.
10. Palade, G. (1973) *Science* **189,** 347–368.
11. Nemoto, T., Kimura, R., Ito, K., Tachikawa, A., Miyashita, Y., Iino, M. & Kasai, H. (2001) *Nat. Cell Biol.* **3,** 253–258.
12. Thorn, P., Lawrie, A. M., Smith, P. M., Gallacher, D. V. & Petersen, O. H. (1993) *Cell* **74,** 661–668.
13. Miller, M. J., Wei, S. H., Parker, I. & Cahalan, M. D. (2002) *Science* **296,** 1869–1873.
14. Nguyen, Q. T., Callamaras, N., Hsieh, C. & Parker, I. (2001) *Cell Calcium* **30,** 383–393.
15. Carrington, W. A., Lynch, R. M., Moore, E. D., Isenberg, G., Fogarty, K. E. & Fay, F. S. (1995) *Science* **268,** 1483–1487.
16. Campos Toimil, M., Edwardson, J. M. & Thomas, P. (2000) *J. Physiol. (London)* **528,** 317–326.
17. Ishihara, Y., Sakurai, T., Kimura, T. & Terakawa, S. (2000) *Am. J. Physiol.* **279,** C1177–C1188.
18. Giovannucci, D. R., Yule, D. I. & Stuenkel, E. L. (1998) *Am. J. Physiol.* **275,** C732–C739.
19. Angleson, J. K., Cochilla, A. J., Kilic, G., Nussinovitch, I. & Betz, W. J. (1999) *Nat. Neurosci.* **2,** 440–446.
20. Buisson, G., Duee, E., Haser, R. & Payan, F. (1987) *EMBO J.* **6,** 3909–3916.
21. Haller, T., Dietl, P., Pfaller, K., Frick, M., Mair, N., Paulmichl, M., Hess, M. W., Furst, J. & Maly, K. (2001) *J. Cell Biol.* **155,** 279–289.
22. Schneider, S. W., Sritharan, K. C., Geibel, J. P., Oberleithner, H. & Jena, B. (1996) *Proc. Natl. Acad. Sci. USA* **94,** 316–321.
23. Schmidt, K., Schrader, M., Kern, H. & Kleene, R. (2000) *J. Biol. Chem.* **276,** 14315–14323.
24. Huttner, W. B. & Zimmerberg, J. (2001) *Curr. Opin. Cell Biol.* **13,** 478–484.
25. Gandhi, S. P. & Stevens, C. F. (2003) *Nature* **423,** 607–613.
26. De Camilli, P., Peluchetti, D. & Meldolesi, J. (1976) *J. Cell Biol.* **70,** 59–74.
27. Jamieson, J. D. & Palade, G. (1971) *J. Cell Biol.* **50,** 135–145.
28. Segawa, A., Loffredo, F., Puxeddu, R., Yamashina, S., Testa-Riva, F. & Riva, A. (1998) *Cell Tissue Res.* **291,** 325–336.
29. Hansen, N. J., Antonin, W. & Edwardson, J. M. (1999) *J. Biol. Chem.* **274,** 22871–22876.